J Solid State Electrochem (2008) 12:1549–1554
DOI 10.1007/s10008-008-0509-3

ORIGINAL PAPER

Effect of different carbon conductive additives on electrochemical properties of $LiFePO_4$-C/Li batteries

Bo Jin · Hal-Bon Gu · Wanxi Zhang · Kyung-Hee Park · Guangping Sun

Received: 11 November 2007 / Revised: 24 December 2007 / Accepted: 30 December 2007 / Published online: 29 January 2008

Abstract $LiFePO_4$-C nanoparticles were synthesized by a hydrothermal method and subsequent high-energy ball-milling. Different carbon conductive additives including nanosized acetylene black (AB) and multi-walled carbon nanotube (MWCNT) were used to enhance the electronic conductivity of $LiFePO_4$. The structural and morphological performance of $LiFePO_4$-C nanoparticles was investigated by X-ray diffraction (XRD) and scanning electron microscopy. The electrochemical properties of $LiFePO_4$-C/Li batteries were analyzed by cyclic voltammetry and charge/discharge tests. XRD results demonstrate that $LiFePO_4$-C nanoparticles have an orthorhombic olivine-type structure with a space group of Pnma. $LiFePO_4$-C/Li battery with 5 wt% MWCNT displays the best electrochemical properties with a discharge capacity of 142 mAh g^{-1} at 0.25 C at room temperature.

Keywords Olivine · Lithium-ion batteries · Hydrothermal method · Carbon conductive additives · High-energy ball-milling

B. Jin · W. Zhang · G. Sun
College of Materials Science and Engineering, Jilin University, Changchun 130025, China

G. Sun
e-mail: sungp@jlu.edu.cn

B. Jin (✉) · H.-B. Gu · K.-H. Park
Department of Electrical Engineering, Chonnam National University, Gwangju 500-757, South Korea
e-mail: jinbo@jlu.edu.cn

Introduction

In the rechargeable lithium-ion batteries, cathode material is a key component mainly devoting to the performance of batteries. Among the known cathode materials, the layered $LiCoO_2$, $LiMnO_2$ and $LiNiO_2$, spinel $LiMn_2O_4$, and other cathode materials including elemental sulfur have been studied extensively [1–9]. Nowadays, $LiCoO_2$ has been utilized as the cathode material for commercial lithium-ion batteries. However, novel cathode material should be developed not only in the field of improving battery performance but also in the field of trying to improve battery safety and reducing its cost.

Recently, lithium transition metal phosphates with an ordered olivine-type structure, $LiMPO_4$ (M=Fe, Mn, Ni, or Co), have attracted great attention due to a high theoretical specific capacity (≈170 mAh g^{-1}) [10, 11, 12]. Among these phosphates, $LiFePO_4$ is the most attractive because of its high stability, low cost and high compatibility with environment [13, 14]. However, it is difficult to attain the full capacity because the electronic conductivity (~10^{-9} S cm^{-1}) is very low, which leads to initial capacity loss and poor rate capability, and diffusion of Li^+ ion in the olivine structure is slow. Many researchers have suggested solutions to this problem as follows: (1) coating with a conductive layer around the particles [15], (2) ionic substitution to enhance the electrochemical properties [16], and (3) synthesis of particles with well-defined morphology [17]. $LiFePO_4$ can be synthesized by various methods such as solid-state reaction method [10], emulsion-drying method [18], co-precipitation method [19], and hydrothermal method [20]. The hydrothermal synthesis is a useful method to prepare fine particles and has some advantages such as simple synthesis process and low energy consumption, compared to

high firing temperature and long firing time during solid-state reaction used conventionally.

High-energy ball-milling process is a promising method for synthesizing cathode materials [21–23]. During the high-energy ball-milling process, the powder particles undergo repeated welding, fracturing, and re-welding in a dry high-energy ball-milling vessel. This results in pulverization and intimate powder mixing [21]. An improvement in electronic conductivity of $LiFePO_4$-C prepared by the high-energy ball-milling process can be expected due to the very fine nanoparticles and their large specific surface area.

In this study, $LiFePO_4$-C nanoparticles were prepared by a hydrothermal method and subsequent high-energy ball-milling. Different carbon conductive additives including nanosized acetylene black (AB) and multi-walled carbon nanotube (MWCNT) were added to improve the electronic conductivity of $LiFePO_4$ nanoparticles. $LiFePO_4$-C/Li batteries were fabricated in an argon-filled glove box, and their electrochemical properties were analyzed by scanning electron microscopy (SEM), X-ray diffraction (XRD), cyclic voltammetry (CV), and charge/discharge experiments.

Experimental

$LiFePO_4$-C nanoparticles were prepared from starting materials of $LiOH{\cdot}H_2O$ (Aldrich, 99.95%), $FeSO_4{\cdot}7H_2O$ (Aldrich, 99%), $(NH_4)_3PO_4{\cdot}3H_2O$ (Wako, 99%), $C_6H_8O_6$ (Aldrich, 99%), nanosized AB (Chevron Chemical, average particle size, 50 nm) or MWCNT (Iljin CNT, purity>95%; length, 10–50 μm; diameter, 10–25 nm). Addition of L-ascorbic acid ($C_6H_8O_6$) as a reducing agent to the precursor was useful in prohibiting the conversion of Fe^{2+} to Fe^{3+} during the hydrothermal reaction and generation of α-Fe_2O_3 during annealing process. $LiOH{\cdot}H_2O$ was dissolved in distilled water. $(NH_4)_3PO_4{\cdot}3H_2O$ and $FeSO_4{\cdot}7H_2O$ powders were added to 1 M LiOH solution in a molar ratio for Li/Fe/P=2.5:1:1. $C_6H_8O_6$ was subsequently added to the above mixture. The resulting mixture was heated at 170 °C for 12 h. After cooling to room temperature, the solution was filtered to separate the precipitated powders; the powders were washed with distilled water. The obtained powders were dried at 110 °C for 1 h under vacuum. To improve low electronic conductivity of $LiFePO_4$, 5 wt% nanosized AB or 5 wt% MWCNT was added into the solution of $LiFePO_4$ nanoparticles and *N*-methylpyrrolidinone (NMP); the mixture was ball-milled for 10 h using a shaker type of ball mill (Planetary Mono Mill) that rotated at 300 rpm. The ball-to-powder weight ratio was 20:1. After drying at 90 °C for 12 h, the powders were pelleted and further heated at 500 °C for 1 h in nitrogen atmosphere. After cooling to room temperature, the mixture of NMP and $LiFePO_4$-C nanoparticles was ball-milled again for 10 h. Finally, the mixture was dried at 90 °C for 12 h.

The crystalline phases were identified with XRD (Dmax/1200, Rigaku) with Cu Kα radiation (λ=1.5406 Å), and powder morphologies were observed by SEM (JEOL JSM-5400).

The composite electrodes were prepared by mixing as-prepared $LiFePO_4$-C with carbon black and polyvinylidenefluoride in a weight ratio of 70:25:5 in NMP. The slurry was coated onto aluminum foil and dried at 90 °C for 1 h before roll-pressing, and then the electrodes were cut into 2×2 cm sections and dried again at 110 °C for 24 h under vacuum. The beaker-type batteries were assembled in an argon-filled glove box using lithium as the anode and 1 M $LiPF_6$ dissolved in ethylene carbonate/dimethyl carbonate (1:1) as the electrolyte. The charge/discharge testing was performed using automatic charge/discharge equipment (WBCS3000, WonATech) in a potential range of 2.0–4.5 V at various C-rates ranging from 0.1 to 10 C (1 C= 170 mA g^{-1}) at room temperature. WBCS3000 battery tester system was also used for measurements of CV at a scan rate of 0.1 mV s^{-1} from 2.0 to 4.5 V. The specific surface area of the samples was measured by the Brunauer, Emmett, Teller method. The electronic conductivity of the samples was measured by a four-point probe method.

Results and discussion

The XRD patterns for $LiFePO_4$-C nanoparticles with different carbon conductive additives are shown in Fig. 1. All the patterns can be indexed to a single-phase material having an orthorhombic olivine-type structure with a space group of Pnma, which is the same as the one that is listed in

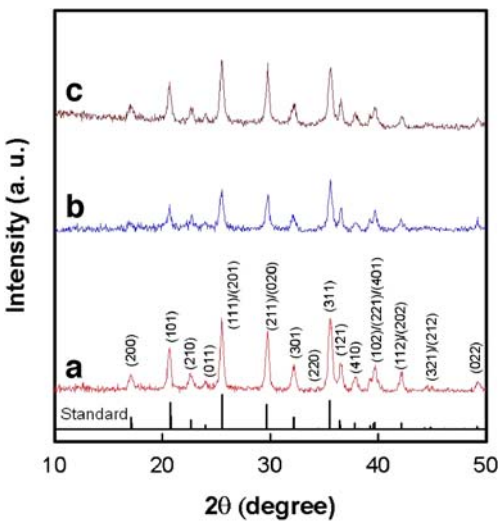

Fig. 1 The XRD patterns for $LiFePO_4$-C nanoparticles with **a** 0 wt%, **b** 5 wt% AB, and **c** 5 wt% MWCNT

the X-ray powder diffraction data file (JCPDS card number 81-1173) by the American Society for Testing Materials that is called standard by us. The crystallite size (D) was calculated by the Scherrer's equation, $D=0.9\lambda/\beta\cos\theta$, from the full-width-at-half-maximum β of five strong and well-resolved reflection peaks corresponding to [200], [101], [210], [011], and [111] crystallographic directions, and the mean value was calculated [24–25]. As shown in Table 1, D value from the Scherrer's equation is 34 nm for $LiFePO_4$, 22 nm for $LiFePO_4$-C with 5 wt% AB, and 19 nm for $LiFePO_4$-C with 5 wt% MWCNT, respectively. It is clear that D value of $LiFePO_4$-C with 5 wt% MWCNT is the smallest. No impurity such as Fe_2O_3, $Li_3Fe_2(PO_4)_3$, and Li_3PO_4 is found in $LiFePO_4$-C powders. There is no evidence for amorphous carbon. It is demonstrated that the added AB or MWCNT does not change crystal structure of $LiFePO_4$ nanoparticles.

The SEM images of $LiFePO_4$-C nanoparticles with different carbon conductive additives are shown in Fig. 2. As shown in Fig. 2a, the average grain size of $LiFePO_4$ nanoparticles is around 50–200 nm in the length and around 20–100 nm in the width. The average grain size of $LiFePO_4$-C with 5 wt% AB is around 100 nm in the length and around 20–50 nm in the width. $LiFePO_4$ nanoparticles are connected each other by amorphous AB. However, in the case of $LiFePO_4$-C with 5 wt% MWCNT, the average grain size is around 50–100 nm. $LiFePO_4$ nanoparticles are connected to each other by amorphous MWCNT. Therefore, the electronic conductivity of $LiFePO_4$-C with 5 wt% AB and 5 wt% MWCNT is improved; as shown in Table 1, 8.00×10^{-5} S cm^{-1} for $LiFePO_4$-C with 5 wt% AB, 1.08×10^{-1} S cm^{-1} for $LiFePO_4$-C with 5 wt% MWCNT, compared to 5.86×10^{-9} S cm^{-1} for $LiFePO_4$. $LiFePO_4$ nanoparticles are much smaller and more dispersed after high-energy ball-milling process. It has been demonstrated that the high-energy ball-milling process provides an effective method in terms of homogeneity and particle size. In particles with a small diameter, lithium ions diffuse over smaller distances between the surfaces and center during lithium intercalation and de-intercalation, and $LiFePO_4$ on the particle surfaces contributes mostly to the charge/discharge reaction. This is helpful to enhance the electrochemical properties of $LiFePO_4$-C/Li batteries due to the increase in the quantity of $LiFePO_4$ nanoparticles that can be used.

Table 1 Properties of $LiFePO_4$-C nanoparticles with different carbon conductive additives

Properties	$LiFePO_4$	$LiFePO_4$-C (5% AB)	$LiFePO_4$-C (5% MWCNT)
Average crystal size (nm)	34	22	19
Electronic conductivity (S cm^{-1})	5.86×10^{-9}	8.00×10^{-5}	1.08×10^{-1}
Specific surface area (m^2 g^{-1})	35.054	53.598	58.244

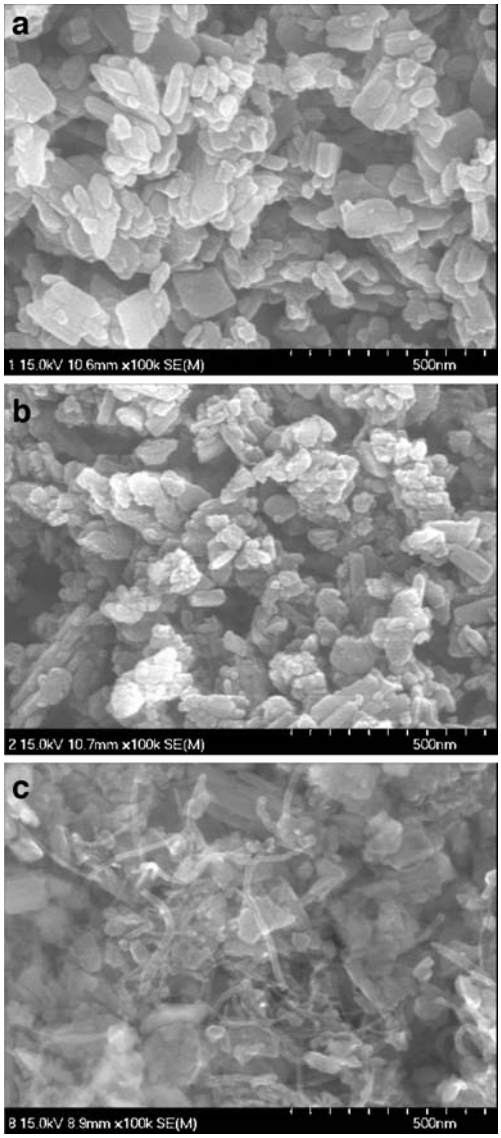

Fig. 2 The SEM images of $LiFePO_4$-C nanoparticles with **a** 0 wt%, **b** 5 wt% AB, and **c** 5 wt% MWCNT

The cyclic voltammograms of $LiFePO_4$-C/Li batteries with different carbon conductive additives are shown in Fig. 3. As for CV, the voltage difference between oxidation peak and reduction peak is an important parameter to value the electrochemical reaction reversibility [23]. As shown in Fig. 3a, oxidation and reduction peaks in the initial cycle appear at around 3.55 and 3.30 V, respectively. The voltage difference between the two peaks is 0.25 V. The oxidation peak decreases and shifts to high potential after six cycles; the corresponding reduction peak also decreases and shifts to low potential. This is due to an increase in the internal

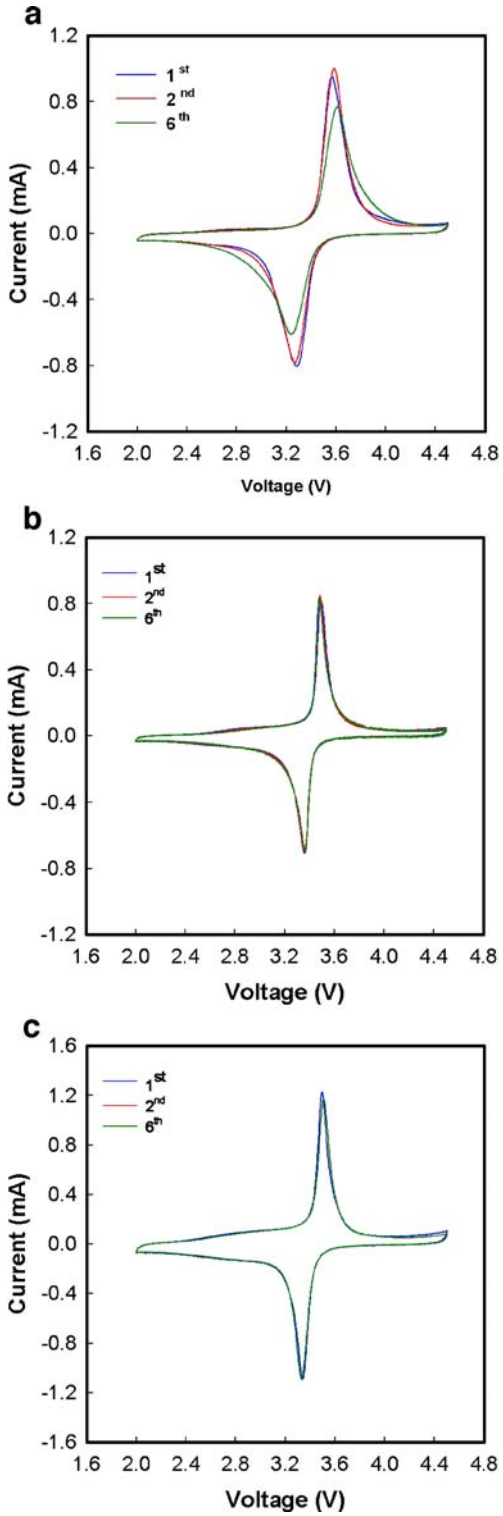

Fig. 3 The cyclic voltammograms of $LiFePO_4$-C/Li batteries with **a** 0 wt%, **b** 5 wt% AB, and **c** 5 wt% MWCNT at a scan rate of 0.1 mV S^{-1}

impedance of battery upon charge/discharge cycling. The oxidation and reduction peaks of $LiFePO_4$-C with 5 wt% AB in the first cycle appear at around 3.49 and 3.37 V, respectively. The voltage difference between two peaks is 0.12 V. The oxidation and reduction peaks hardly shift to high or low potential after six cycles. However, in the case of $LiFePO_4$-C with 5 wt.% MWCNT, the oxidation and reduction peaks in the initial cycle appear at around 3.48 and 3.34 V, respectively. The voltage difference between two peaks is 0.14 V. The oxidation and reduction peaks hardly shift to high or low potential after six cycles. The intensities of oxidation and reduction peaks for $LiFePO_4$-C/Li battery with 5 wt% MWCNT are the largest. Meanwhile, the redox peak profiles of $LiFePO_4$-C/Li batteries with 5 wt% AB and 5 wt% MWCNT are more symmetric and spiculate than that of $LiFePO_4$/Li battery. This demonstrates that the reversibility and reactivity of $LiFePO_4$-C/Li battery are better than that of $LiFePO_4$/Li battery.

The initial discharge curves of $LiFePO_4$-C/Li batteries with different carbon conductive additives at various C-rates ranging from 0.1 to 10 C (1 C=170 mA g^{-1}) are shown in Fig. 4. The batteries were charged/discharged several times at 0.2 °C, and then the charge/discharge tests at various C-rates in a potential range of 2.0–4.5 V were performed. The characteristic flat discharge plateau at around 3.4 V, which represents a two-phase reaction in the electrode, is observed for three samples. As shown in Fig. 4a, the initial discharge capacity of $LiFePO_4$/Li battery is 167 mAh g^{-1} at 0.1 C close to the theoretical capacity of $LiFePO_4$ (170 mAh g^{-1}), 138 mAh g^{-1} at 0.3 C, 127 mAh g^{-1} at 0.5 C, 111 mAh g^{-1} at 1 C, 75 mAh g^{-1} at 3 C, 53 mAh g^{-1} at 5 C, and 26 mAh g^{-1} at 10 C, respectively. The potential plateau remains flat even for the 1 C curve except for a slight decrease. The initial discharge capacity of $LiFePO_4$-C/Li battery with 5 wt% AB is 136 mAh g^{-1} at 0.1 C, 125 mAh g^{-1} at 0.3 C, 120 mAh g^{-1} at 0.5 C, 112 mAh g^{-1} at 1 C, 96 mAh g^{-1} at 3 C, 88 mAh g^{-1} at 5 C, and 72 mAh g^{-1} at 10 C, respectively. The potential plateau remains flat even for the 10 C curve except for a slight decrease. However, in the case of $LiFePO_4$-C/Li battery with 5 wt% MWCNT, the initial discharge capacity is 143 mAh g^{-1} at 0.1 C, 131 mAh g^{-1} at 0.3 C, 128 mAh g^{-1} at 0.5 C, 121 mAh g^{-1} at 1 C, 104 mAh g^{-1} at 3 C, 95 mAh g^{-1} at 5 C, and 76 mAh g^{-1} at 10 C, respectively. The potential plateau remains flat even for the 10 C curve except for a slight decrease. On the basis of above results, it is concluded that the battery can operate at relatively high rates up to 10 C, confirming the improved kinetics of $LiFePO_4$-C nanoparticles. Meanwhile, it is also demonstrated that the discharge rate capability of $LiFePO_4$-C/Li battery with 5 wt% AB and 5 wt% MWCNT is better than that of $LiFePO_4$/Li battery; this is due to the increase in electrical conductivity and specific surface area and decrease in average crystal size when adding 5 wt% AB or 5 wt% MWCNT, as demonstrated in Table 1. $LiFePO_4$-C with 5 wt% MWCNT displays the best initial discharge rate performance between two $LiFePO_4$-C samples, and this is

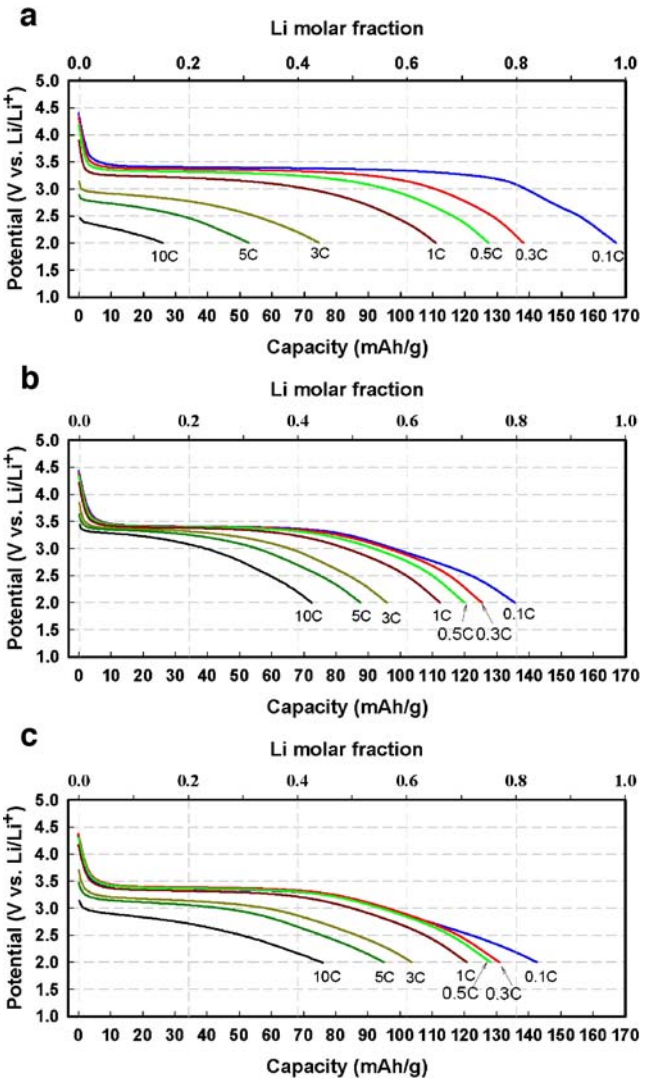

Fig. 4 The initial discharge curves of $LiFePO_4$-C/Li batteries with **a** 0 wt.%, **b** 5 wt% AB, and **c** 5 wt% MWCNT at various C-rates ranging from 0.1 to 10 C (1 C=170 mA g^{-1})

due to the largest electronic conductivity, the largest specific surface area, and the smallest crystal size, as demonstrated in Table 1, which is consistent with the XRD results in Fig. 1 and CV in Fig. 3. It is clear that the initial discharge capacity decreases with increasing C-rate. This phenomenon can be explained in terms of the electric polarization due to an increase in the *IR* drop, where *I* is the current passing the battery and *R* is the battery impedance.

The cycling performance of $LiFePO_4$-C/Li batteries with different carbon conductive additives at a discharge rate of 0.25 C is shown in Fig. 5. The charge/discharge tests at various C-rates ranging from 0.1 to 10 C (1 C= 170 mA g^{-1}) were performed, and the results are shown in Fig. 6. The batteries were tested between 2.0 and 4.5 V. As shown in Fig. 5a, the discharge capacity of $LiFePO_4$/Li battery is 143 mAh g^{-1} at the first cycle and decreases to

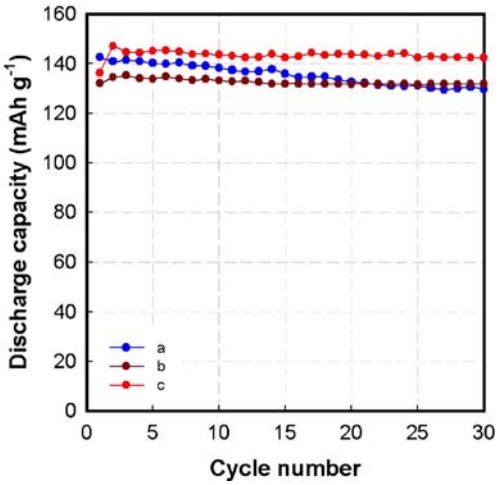

Fig. 5 The cycling performance of $LiFePO_4$-C/Li batteries with **a** 0 wt%, **b** 5 wt% AB, and **c** 5 wt% MWCNT at 0.25 C

130 mAh g^{-1} after 30 cycles. It is clear that the discharge capacity decreases upon cycling. $LiFePO_4$-C/Li battery with 5 wt% AB has a stable discharge capacity of 132 mAh g^{-1} until 30 cycles. $LiFePO_4$-C/Li battery with 5 wt% MWCNT exhibits the best cycling performance with a discharge capacity of 142 mAh g^{-1}, which is consistent with the XRD results in Fig. 1 and CV in Fig. 3. This depends on the largest electronic conductivity, the largest specific surface area, and the smallest crystal size, as demonstrated in Table 1. Figure 6 also demonstrates that $LiFePO_4$-C/Li battery with 5 wt% MWCNT has the best cycling performance.

Conclusions

$LiFePO_4$-C nanoparticles have been synthesized successfully by a hydrothermal method and subsequent high-

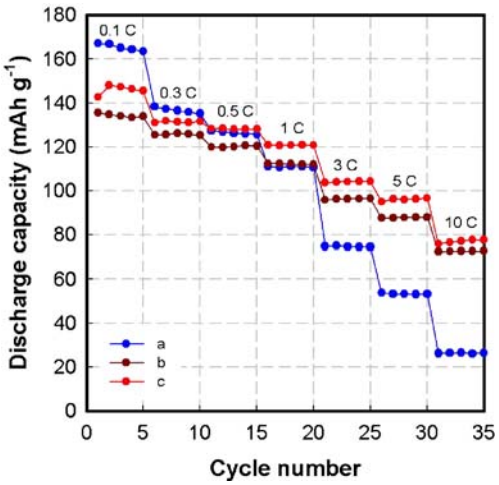

Fig. 6 The cycling performance of $LiFePO_4$-C/Li batteries with **a** 0 wt%, **b** 5 wt% AB, and **c** 5 wt% MWCNT at various C-rates ranging from 0.1 to 10 C (1 C=170 mA g^{-1})

energy ball-milling. Different carbon conductive additives including AB and MWCNT were used to enhance the electronic conductivity of $LiFePO_4$. The XRD results demonstrate that $LiFePO_4$-C nanoparticles have an orthorhombic olivine-type structure with a space group of Pnma. $LiFePO_4$-C/Li battery with 5 wt% MWCNT displays the best electrochemical properties with a discharge capacity of 142 mAh g^{-1} at 0.25 C at room temperature.

Acknowledgments This research project received supporting funds from the second-stage Brain Korea 21.

References

1. Pistoia G, Zane D, Zhang Y (1995) J Electrochem Soc 142:2551
2. Resimers JN, Dahn JR, von Sacken U (1993) J Electrochem Soc 140:2752
3. Li W, Resimers JN, Dahn JR (1993) Solid State Ionics 67:123
4. Dahn JR, von Sacken U, Juzkow MW, Al-Janaby H (1991) J Electrochem Soc 138:2207
5. Koetschau I, Richard MN, Dahn JR, Soupart JB, Rousche JC (1995) J Electrochem Soc 142:2906
6. Jeong I-S, Kim J-U, Gu H-B (2001) J Power Sources 102:55
7. Jin B, Kim J-U, Gu H-B (2003) J Power Sources 117:148
8. Kim J-U, Jo Y-J, Park G-C, Gu H-B (2003) J Power Sources 119–121:686
9. Jin B, Jun D-K, Gu H-B (2006) Trans Electr Electron Mater 7:76
10. Padhi AK, Nanjundaswamy KS, Goodenough JB (1997) J Electrochem Soc 144:1188
11. Bramnik NN, Bramnik KG, Buhrmester T, Baehtz C, Ehrenberg H, Fuess H (2004) J Solid State Electrochem 8:558
12. Jin B, Gu H-B, Kim K-W (2008) J Solid State Electrochem 12:105
13. Shiraishi K, Dokko K, Kanamura (2005) J Power Sources 146:555
14. Myung ST, Komaba S, Hirosaki N, Yashiro H, Kumagai N (2004) Electrochimica Acta 49:4213
15. Yun NJ, Ha H-W, Jeong KH, Park H-Y, Kim K (2006) J Power Sources 160:1361
16. Chung S-Y, Bloking JT, Chiang Y-M (2002) Nat Mater 1:123
17. Yamada A, Chung SC, Hinikuma K (2001) J Electrochem Soc 148:A224
18. Cho T-H, Chung H-T (2004) J Power Sources 133:272
19. Yang M-R, Ke W-H, Wu S-H (2005) J Power Sources 146:539
20. Franger S, Cras FL, Bourbon C, Rouault H (2005) J Power Sources 119–121:252
21. Jeong W-T, Lee KS (2002) J Power Sources 104:95
22. Rabanal ME, Gutierrez MC, Garcia-Alvarado F, Gonzalo EC, Arroyo-de Dompablo ME (2006) J Power Sources 160:523
23. Ni JF, Zhou HH, Chen JT, Zhang XX (2005) Mater Lett 59:2361
24. Sanchez MAE, Brito GES, Fantini MCA, Goya GF, Matos JR (2006) Solid State Ionics 177:497
25. Arnold G, Garche J, Hemmer R, Strobele S, Volger C, Wohlfahrt-Mehrens M (2003) J Power Sources 119–121:247